Research Article

Studying on mineralogical characteristics of a refractory high-phosphorous oolitic iron ore

Xiao Junhui[1,2,3] · Zou Kai[1] · Wang Zhen[1]

Received: 17 March 2020 / Accepted: 3 May 2020 / Published online: 9 May 2020

Abstract
In this study, a high-phosphorus oolitic iron ore containing 44.70% Fe and 1.56% P from western Hubei of China was collected as the sample. The chemical composition, mineral composition, structure characteristics, dissemination characteristics, and iron and phosphorus occurrence state were carried out to investigate the mineralogical characteristics of the high-phosphorus oolitic iron. The results show that the high-phosphorus oolitic iron ore is a chemical sedimentary iron ore, mainly composed of oolite (more than 60%). Specifically, the ooids consists of oolite nuclei, collophanite girdles, and hematite and limonite girdles; the detritus is composed of fine-grained hematite and quartz feldspar; and cement is composed of carbonate minerals and worm-like hematite. The iron concentrate consists of iron-rich oolite and some hematite. The iron-bearing minerals in the oolite are mainly hematite, limonite, chlorite, and collophanite, and a close relationship between the hematite-limonite in the oolites and the iron-containing chamoisite can be observed. Upgrading iron and removing phosphorus from the high-phosphorus oolitic iron ore will be difficult by physical beneficiation.

Keywords High-phosphorous oolitic iron ore · Occurrence state · Hematite-limonite · Collophanite

1 Introduction

Oolitic hematite generally forms large sedimentary iron ore deposits, such as those in the underground iron mines of France (Lorraine), and in the United States (Clinton) [1–3]. Oolitic hematite, as its name suggests, is characterised by its oolitic structure, leading to the fine dissemination of grains. During the process of mineralisation, hematite-limonite, quartz, and clay gangue minerals are generally wrapped in irregular shell-like layers from the centre of the oolite, forming a multi-layered structure [4, 5], where no obvious boundary exists between the iron mineral layers and gangue layers, but there is a transitional distribution, in addition to the fine dissemination of grains of the iron mineral and gangue minerals in such iron ores. With the degree of dissociation of iron mineral monomers of 85%, the common diameter of mineral particles is up to about 20 μm, which has been beyond the ability of current beneficiation equipment, and has led to difficulty in the separation of oolitic hematite [5–7]. Major producing areas of high-phosphorus oolitic iron ore are distributed in North America, Northern Europe, Australia, Saudi Arabia, and the Yangtze River region in China [6–8]. These phosphorus-containing weakly magnetic iron ores can be divided into hydrothermal iron ores and sedimentary iron ores. The phosphorus in the former type mainly exists in the form of apatite, whereas that in the latter type mainly exists in the form of oolitic collophanite, and a close relationship can be found between these minerals and iron minerals [9–11].

In addition, these minerals are often attached to the edge of iron oxide mineral particles, or are embedded in

✉ Xiao Junhui, xiaojunhui33@163.com | [1]Sichuan Provincal Engineering Laboratory of Non-Metallic Mineral Powder Modification and High-Value Utilization, Southwest University of Science and Technology, Mianyang 621010, China. [2]The State Key Laboratory of Refractories and Metallurgy, Wuhan University of Science and Technology, Wuhan 030192, China. [3]Key Laboratory of Ministry of Education for Solid Waste Treatment and Resource Recycle, Southwest University of Science and Technology, Mianyang 621010, China.

SN Applied Sciences (2020) 2:1051 | https://doi.org/10.1007/s42452-020-2871-4

quartz or carbonate minerals, with a small amount of iron minerals in the lattice of iron minerals [12–14]. Apatite crystals, mainly in pillar, acicular, or aggregated shapes or in the form of dispersed particles, are embedded in iron minerals and gangue minerals, and are characterised by their fine granularity. Some are refractory iron ores with granularity of less than 2 μm, resulting in difficulty in their separation [15–18].

From 2008 to 2018, China's iron and steel industry continued to increase its iron ore external dependence, reaching more than 60%. In order to support the rapid growth of steel output, the amount of iron ore, the main raw material of iron making, must also increase rapidly. Oolitic hematite is an important potential iron ore resource. There are about 4 billion to 5 billion tons of reserves in China, about 14 billion tons of reserves in Europe, and corresponding resources have been reported in the United States, Egypt and other countries. However, a large number of high phosphorus iron ore has not been used. The high phosphorus iron ore of phosphorus mainly fluorapatite form apatite or carbon and other mineral paragenesis, disseminated in iron ore particles of edge, embedded throughout silica or carbonate minerals, a small amount of occurrence in iron content in the lattice, and apatite disseminated extent is smaller, some even under 2 m (including physical separation method is difficult to separate, belongs to the ore difficult to choose. However, China's high-phosphorous iron ore has a high grade of raw ore iron (the mass fraction is about 45%, far higher than the average iron grade of China's iron ore 32.6%, large reserves (accounting for 14.86% of the total reserves, about 7.45 billion therefore, it is of great significance to solve the problem of the utilization of high-phosphorous iron ore to solve the supply of iron ore resources and the development of iron and steel industry in China.

Because oolitic hematite embedded fine grain, In order to make its monomer dissociation, fine grinding is required. It is difficult to recover iron and decrease phosphorus using conventional methods. At present, the iron ore processing process as follows:

1. Shaft furnace roasting

The shaft furnace that roasts hematite ore for mineral processing is a large-scale industrial kiln, which can be categorized as thermal equipment. It is used to turn weak-magnetic mineral ore into strong-magnetic ore through a technical process named magnetization roasting. The magnetization roasting process of hematite or specularite ore inside the shaft furnace can be divided into four phases, namely, the orefeeding, ore preheating, heating, reduction, cooling and discharge.

2. Rotary kiln roasting

With the slow rotation (0.4 -1.0 r/m) of the rotary kiln, the hematite or specularite within iron ores are first heated in countercurrent with the hot off-gas from the burner, and then reduced to magnetite by reducing gas CO, which is generated from the Boudouard reaction. Namely, when solid reducing agents (such as coal) were used, CO_2 generated in the reduction reactions subsequently reacted with the solid carbon to produce more CO. Boudouard reaction is an endothermic reaction, which means increasing temperature enables the Boudouard reaction to occur as fast as possible, thus causing a high CO partial pressure and an accelerated magnetic reduction of hematite or specularite.

3. Fluidized bed roasting

In the fluidized bed furnace, the solid material to be roasted is shaken up by an upward current of gas which maintains the individual particles in suspension. Precise adjustment of the velocity of the gas to the grain size and the specific weight of the material to be roasted makes it possible to generate a floating mixture of gas and solids which behave almost like a liquid. The process is reported to have the following advantages over the other roasting techniques: ease of control due to absence of moving parts within the reactor, homogeneity of discharge products, ability to handle fine particles (<0.8 mm) and high efficiency of heat transfer and mass transfer.

4. Microwave assisted roasting

Microwave roasting is a new field of magnetization roasting research. It is unique and different from conventional heating. Microwave is a non-ionizing form of electromagnetic wave with frequency ranging from 300 MHz to 300 GH, which can be absorbed by dielectrics. Thus, microwave radiation roasting is also referred to as dielectric heating. The interaction of dielectric minerals (such as siderite, hematite, limonite and pyrite) with microwave radiation results in dielectric minerals heating due to the ionic conduction and dipolar rotation in dielectric minerals induced by alternating microwave electromagnetic field. Compared with conventional roasting techniques (shaft furnace roasting, rotary kiln roasting et al.), microwave radiation roasting is unique and offers a number of advantages such as rapid heating, noncontact heating, material-selective heating, volumetric heating and nonpollution. Furthermore, findings of recent investigations revealed that microwave assisted heating had a significant influence on the magnetic properties of iron ores, such as hematite, pyrite, ilmenite, and siderite [19].

Therefore, it is of great practical significance for this study to carry out mineralogical research on high-phosphorus iron ore in Hubei province of China and provide mineralogical research guidance for the exploitation of high-phosphorus iron ore resources in this region.

2 Materials and method

2.1 Sampling

In Badong County, Hubei Province, the morphology of high-phosphorus oolitic iron ore body is mainly influenced by sedimentary environment. According to the engineering control, orebody lying in the long axis of the north shows the belt shape in the northeastern direction. The northwest side of the orebody, due to its location in the sedimentary margin, shows irregular wavy shape. The southeast side of the orebody boundary, compared with that of Dengjia, Kuangdong and Jinshi, is presumed to extend to the southeast. The orebody occurrence is generally influenced by the shape of Hejiaping anticline. The southeastern wing of the anticline is in the shape of a half-box fold from Taohua to Fengzhuping. The northwestern side of half-box folded orebody is gently inclined, while the southeastern side is inclined steeply. The orebody occurrence is consistent with that of strata. The dip angles of the northwester wing and the southeastern wing of the gently inclined orebody are 10°–25°and 10°–30° respectively. And the dip angle of steep inclined orebody is more than 80°, with some parts inversed. Resources of orebody: In 2006 and 2007, the gently inclined orebodies of 331, 332 and 333 contain 22.3 million, 26.42 million and 5.96 million tons of resources respectively, with a total of total of 54.68 million tons; and the steeply inclined orebody of 333 contains 12.27 million tons. The total amount of various resources in the orebody is 66.75 million tons. In 2008, 40.93 million tons of resources will be anticipated. Therefore, with a total amount of 1076.8 million tons of resources, this orebody is considered as a large ore body [20, 21].

The experimental sample was some sort of High-Phosphorous Oolitic Iron Ore from Badong County of western Hubei Province, collected by using groove sampling method from the underground tunnel, with particle size in the range of 150–0 mm (part of 200 mm). The sample was crushed by double–roll crusher to less than 30 mm after coarse crushing, fine-crushing and division.

2.2 Methods

The chemical composition of solid materials was analyzed by Z-2000 atomic absorption spectrophotometer (Hitachi Co., Ltd.), the diffraction grating was Zenier-tana Type, 1800 lines /mm, the flash wavelength was 200 nm, the wavelength range was 190– 900 nm, the automatic peak seeking setting, and the spectral bandwidth was divided into 4 grades (0.2, 0.4, 1.3, and 2.6 nm) for the analysis of mineral chemical composition. The phase composition of solid substances was analyzed by X-ray diffraction (XRD, X Pert pro, Panaco, The Netherlands). The microstructure of the solid products was observed by SEM (S440, Leica Cambridge LTD, Germany) equipped with an energy dispersive X-ray spectroscopy (EDS) detector (Ultra55, CarlzeissNTS GmbH, Germany). Polarised light microscopy was performed using a BK-POL reflected polarising microscope produced by Chongqing Optec Instrument Co., Ltd, and chemical composition was analysed by means of polarised light microscopy, mineral phase, energy spectrum, and electron probe analysis. Electron probe microanalysis (EMPA) was used to determine the contents of major elements of distinguishable single minerals in the ore samples. The instruments used for examination include electronic probe microscopic analyzer (EPMA) plus energy disperse spectroscopy (Mode: J XA-8230/INCAX-ACT) produced by JEOL Ltd.

3 Results and discussion

3.1 Mineral composition

3.1.1 Minerals

The main mineral found in the ore is hematite, which accounts for more than 90% of the ore, and a few siderites can occasionally be found. Hematite belongs to the trigonal system of oxide minerals, and exists either in cryptocrystalline form or in the form of oolite. The granularity of the oolite generally ranges from 0.15 to 0.80 mm, typically around 0.45 mm. Some oolites consist of non-(hidden) crystalline hematite, and no significant circular structure can be observed, whereas others are characterised by a girdle structure with hematite at the core, and chlorite and hematite are sometimes wrapped together on the outer layer. Compound oolites, which account for about two-thirds of the total, generally occur in 3–7 layers, where the thickness of each layer is less than 0.01 mm. Most oolites are composed of non-(hidden) crystalline hematite. The phase analysis results are as follows: more than 98.86% hematite and <0.39% iron silicate. Siderite, occasionally found in the ore, is a mineral composed of rhombic crystal system carbonate, mostly existing in the form of automorphic crystals. It is characterised by its fine and even granularity of <0.05 mm. Siderite is commonly embedded in the hematite matrix, and comprises less than 0.57% according to the phase analysis results.

3.1.2 Gangue minerals

The gangue minerals in the ore are mainly quartz, with calcite, dolomite, chlorite, hydromica, and collophanite. The quartz represents terrigenous clasts, mostly sub-angular in shape, with granularity distributed in the 0.015–0.23 mm range, generally around 0.075 mm. It is extremely unevenly distributed in the ores, sometimes existing in the form of strips; they are mostly scattered in cryptocrystalline hematite, although a few are dispersed in calcite, or cemented with calcite, quartz, dolomite, and other hybrids in hematite oolites. The proportion of SiO_2 contained in the ore is less than 13.41%. The calcite mostly exists in the form of automorphic crystal particles, generally with granularity of 0.045–0.075 mm. Some of these particles are cemented by aphanitic hematite, whereas others, with contents of less than 5%, are cemented into the oolitic hematite with quartz. Chlorite is mainly distributed in the oolitic layers, whose thickness is generally less than 0.01 mm, although some chlorite crystals are distributed in the pores of the cement, with contents of less than 0.5%. Hydromica is sparsely distributed in the iron ore matrix, existing in the form of microscopic lepidosomes with a granularity of less than 0.005 mm. Collophanite is an amorphous mineral that is radial and granular in shape, and exists in isolated irregular massive form, where the quartz and hematite particles are often wrapped, with a grain size of 0.2–1.2 mm. The collophanite sometimes forms layered oolite with hematite, with a few thin layers. Pyrite was sparse in the iron ore; only one or two pieces of anhedral pyrite with granularity of less than 1 mm were observed.

3.1.3 Structure and shape

(1) Structure

The ore is mainly characterised by a bean oolitic structure (in Fig. 1) and oolitic sand structure. The bean oolitic structure is a concentric girdle with an alternating arrangement of certain amounts of chlorite, hydromica, dolomite, and hematite, and is round, sub-rounded, and oval in shape,respectively. Ambiguous surface or lepidocrocite reaction can occasionally be observed because of the recrystallisation effect. There are also a few quartz, siderite, magnetite, gravel, and chert particles filled between these particles. The granularity of the ore with bean oolitic structure generally ranges from 1 to 3 mm, with oolites 0.6–0.8 mm in size, whereas the gravel is larger than 15 mm. The ore exists in the form of a porous cemented structure that is particle-supported.

Oolitic sand structure: Oolite with homocentric layers is formed by hematite associating with hydromica, chlorite, and other components of mudstone, but no internal structure can be observed. A few quartz grains are sub-angular or sub-circular in shape, siderite is characterised by its automorphic shape, and most chert is irregular and massive. Magnetite is irregular compared with hematite, and is characterised by its uneven distribution and general granularity distribution in the 0.6–1.3 mm range.

(2) Shape

The shape is mainly divided into banded and massive shapes. Some ores in the banded shape often appear at the top of the ore body, and are composed of hematite strips and purple-red iron powder-containing sandy and muddy strips, whereas others appear in the lower part of the ore body, and consist of purplish-red thin muddy layers with lenticular and layered hematite. The massive ore shape is distributed in the middle of the ore body, characterised by its bean structure in the middle and upper parts, and oolitic and sandy colloidal structure in the middle and lower parts.

3.1.4 Chemical composition

The main chemical composition analysis results for the crude ore are shown in Table 1, the iron phase analysis results for the crude ore are shown in Table 2, and the

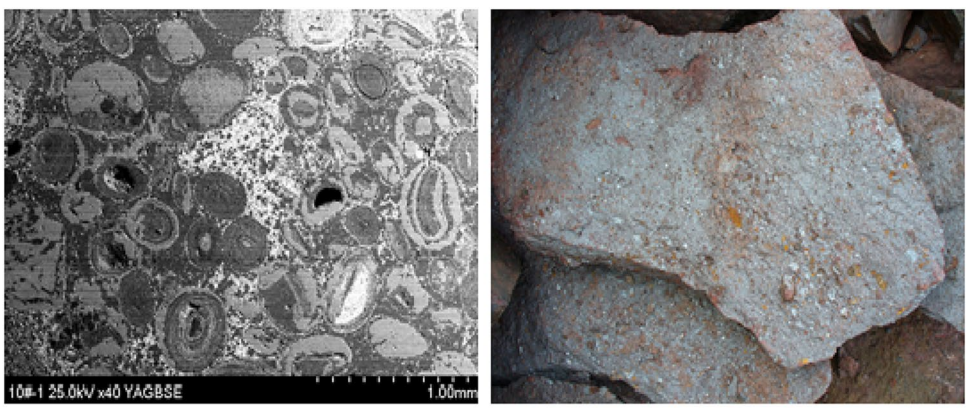

Fig. 1 Hematite (**a** hematite with oolitic structure; **b** massive hematite ore with bean oolitic structure)

Table 1 Main chemical composition of the crude ore (wt.%)

TFe	P	S	F	SiO_2	Al_2O_3	CaO	K_2O	Na_2O	C	H_2O^+	V_2O_5	MgO
44.70	1.56	0.05	0.16	13.58	6.56	5.63	0.40	0.071	0.86	2.89	0.091	1.26

Table 2 Iron phase analysis of the crude ore (wt.%)

TFe	Magnetite	Iron oxide	Siderite	Pyrite	Ferrosilite
44.976	0.041	43.980	0.690	0.105	0.160

results for the main mineral composition, granularity, and contents are shown in Table 3.

3.2 Dissemination characteristics of crude ore minerals

3.2.1 Hematite

For single-crystal hematite and hematite aggregates, the granularity of hematite aggregates in the ore was 0.002–0.5 mm, and hematites with grain sizes of more than 0.1 mm were few; 80% were smaller than 0.074 mm. These hematite were relatively pure, accounting for 9.35% in the ore. SEM images and the EDS composition analysis of hematite in the oolite are shown in Fig. 2, and the electron probe composition of the hematite is shown in Table 4.

The average content of FeO in the hematite accounted for 89.00%, whereas the mineral contents of single-crystal hematite and hematite aggregates in the ores only accounted for 9.35%, with 80% of the grains smaller than 0.074 mm, but the minerals were relatively pure, with high iron contents and granularity within the effective magnetic separation and flotation range, which plays an important role in improving iron ore grade.

Table 3 Composition, granularity, and contents of sample

Type	Minerals	Granularity(mm)			Content (wt.%)
		Min	Max	Average	
Sulfide	Pyrite	0.002	1	0.03–0.2	0.24
Metallic minerals	Magnetite	0.01	1	0.05–0.35	0.34
	Hematite	0.002	0.8	0.01–0.5	9.35
	Hematite-Limonite	0.02	0.5	0.05–0.25	62.65
	Siderite	0.001	1	0.01–0.3	1.15
Gangue minerals	Chlorite(clay mineral)	0.001	0.08	0.005–0.05	9.66
	biotite	0.05	1	0.1–1.5	0.54
	Calcite	0.05	1	0.1–0.4	0.87
	Dolomite	0.05	1.5	0.1–0.3	0.64
	Quartz	0.05	0.3	0.11	8.36
	feldspar	0.005	1.5	0.02–0.1	0.97
Chlorite	Collophanite	0.05	0.6	0.1–0.3	5.23

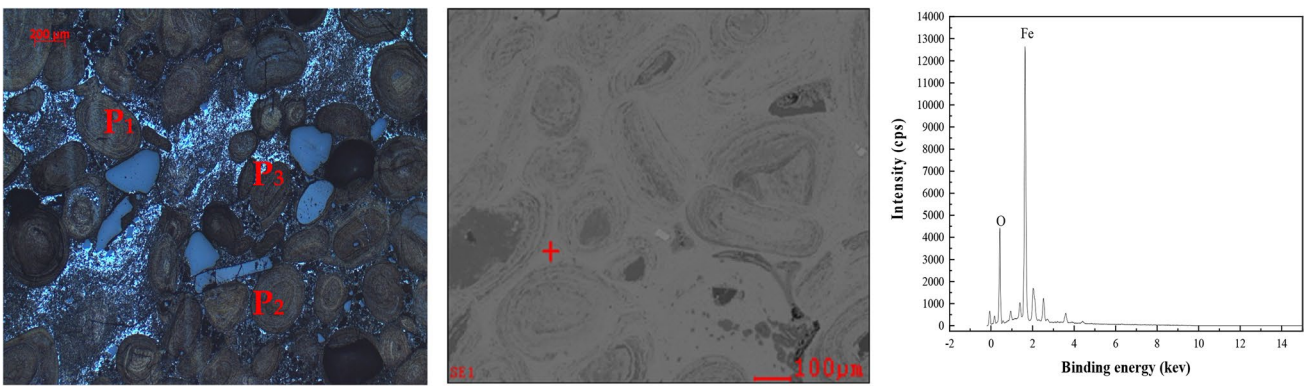

Fig. 2 SEM images and EDS composition analysis of hematite in oolite

Table 4 Electron probe composition of the hematite (wt.%)

Position	Al_2O_3	SiO_2	FeO	MgO	CaO	Totals
P_1	0.811	0.969	88.890	0.013	0.082	90.765
P_2	0.841	0.955	88.822	0.003	0.081	90.702
P_3	0.927	0.877	89.283	0.001	0.072	91.16
Average	0.859	1.004	88.998	0.005	0.078	90.944

Table 5 Chemical compositions of oolite, iron-rich oolite, and lean-iron oolite (%)

Minerals	Fe	FeO	P_2O_5
Oolite	48.34	3.65	3.49
Iron-rich oolite	51.19	3.09	3.03
Lean-iron oolite	41.80	0.00	3.92

3.2.2 Hematite-limonite

In addition to the 9.35% of single crystal hematite and hematite aggregates in ores, 62.65% is composed of hematite, chlorite, limonite, and clay to form oolite. The oolite, the main component of the ores, is composed of hematite, chlorite, and a small amount of collophanite in the chemical sedimentary crude iron ores. Hematite and chlorite in the oolite are characterised by their fine granularity and close dissemination.

The original state of the oolite formed in the iron ore was basically maintained because of the lack of crustal movement and later magmatic transformation. In terms of the process, the oolite, mainly composed of hematite-limonite, was the main target for iron selection. Because the oolitic particles with granularity larger than 0.1 mm account for more than 90%, the fineness of the grinding can be reduced, contributing to reduced loss of mud yield and iron.

(1) Average iron content in hematite-limonite.

Most hematite-limonite occurs in the oolite, where a quartz nucleus can be found in most ooids. The chemical compositions of the oolite, iron-rich oolite, and lean-iron oolite (%) are shown in Table 5.

Most quartz nuclei in these oolites can be dissociated by monomers after being broken up. A representative ooid in the ore was tested by means of electron probe analysis to measure the iron content. The electron probe composition of hematite-limonite (%) is shown in Table 6. The results show the hematite-limonite accounting for 62.65% of the ore taken as a target for separation, and its theoretical iron ore grade is up to 56.19%.

(2) Occurrence state of hematite-limonite in oolites.

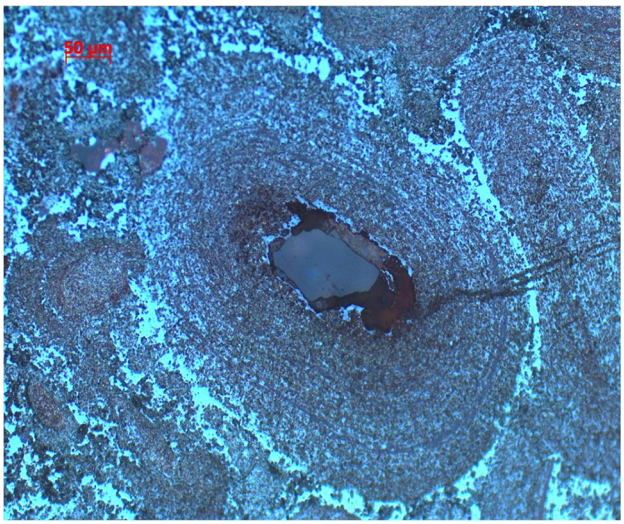

Fig. 3 Oolite with quartz nuclei

Table 6 Electronic probe composition of hematite-limonite (wt.%)

Position	TiO_2	MgO	SiO_2	Al_2O_3	CaO	K_2O	MnO	Fe
P_4	0.11	0.91	9.59	7.79	0.02	0.00	0.00	60.37
P_5	0.15	0.52	7.51	5.43	0.11	0.00	0.03	63.83
P_6	0.19	0.75	7.84	5.69	0.72	0.00	0.00	62.76
P_7	0.03	2.85	18.97	17.47	0.12	0.00	0.09	44.74
P_8	0.12	2.08	16.25	39.8	2.22	0.00	0.00	29.27
P_9	0.19	0.14	4.35	2.98	0.05	0.00	0.04	68.27
P_{10}	0.08	1.5	13.52	13.73	0.26	0.00	0.01	52.47
P_{11}	0.18	0.34	4.53	3.17	0.09	0.00	0.00	67.85
Average	0.13	1.14	10.32	12.01	0.45	0.00	0.02	56.19

The hematite-limonite in the form of oolite accounts for 64.26% of the total ore sample. Thus, the morphology of hematite in the oolite, the granularity of single-crystal hematite and aggregates, and the dissemination characteristics of other minerals including quartz (Fig. 3), collophanite, and chlorite have strong influence on beneficiation. The hematite-limonite in oolites with concentric and oval particle shapes is closely embedded with limonite, chlorite, collophanite, dolomite, and clay minerals, which have fine granularity of 0.X–100 μm. Among them, hematite is commonly found, for which granularity of larger than 20 μm may account for 20%.

According to the characteristics of the oolites observed under the microscope (Fig. 4), unevenly distributed iron minerals, which are composed of hematite and limonite in the oolite, can be found; under the microscope, some oolites were hard and dark brown in colour, whereas some were loose and brown. Oolite, iron-rich oolite, and lean-iron oolite were randomly chosen for chemical analysis, and the results show that the difference in iron content between iron-rich oolite and lean-iron oolite is close to 10%.The element surface scan images of iron-rich oolite and lean-iron oolite in Fig. 5 show that many oolites have hematite cores. In addition, hematite and quartz, as well as collophanite, are distributed in the oolites.

(3) Mineral distribution of iron in oolites.

The iron-bearing minerals in the oolites are mainly hematite, limonite, chlorite, and collophanite. As shown in Fig. 6, the upper part represents FeO, whereas the lower part shows collophanite. The SEM and EDS images of the components show that the positions and homogeneity of Fe, Si, and O are consistent with the mixture of hematite-limonite and chlorite, and a close relationship between the hematite-limonite in the oolite and the iron-bearing chlorite.

The scanning electron microscopy results show that the electron image is consistent with the observation and analysis under the microscope. ($FeOOH{\cdot}H_2O$), Goethite, esmeraldite, lepidocrocite and hydrolepidocrocite, water-rich iron hydroxide gelation, aluminium hydroxides, water-containing oxides, and mud often occur together.

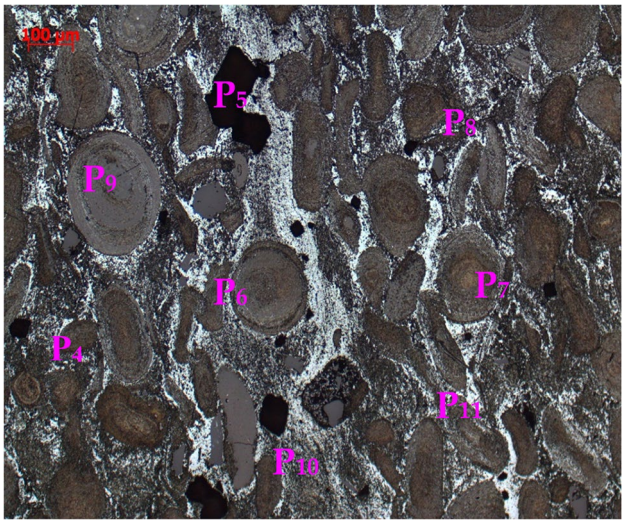

Fig. 4 Iron-rich oolite and lean-iron oolite cemented

3.2.3 Magnetite

Magnetite is composed of FeO (31.03%), Fe_2O_3 (68.97%), or Fe (72.40%), and O_2 (7.60%). Fe_3 is often replaced by AL, V, or Cr, and Fe_2 is easily replaced by Mg, Ni, Co, or Zn in this

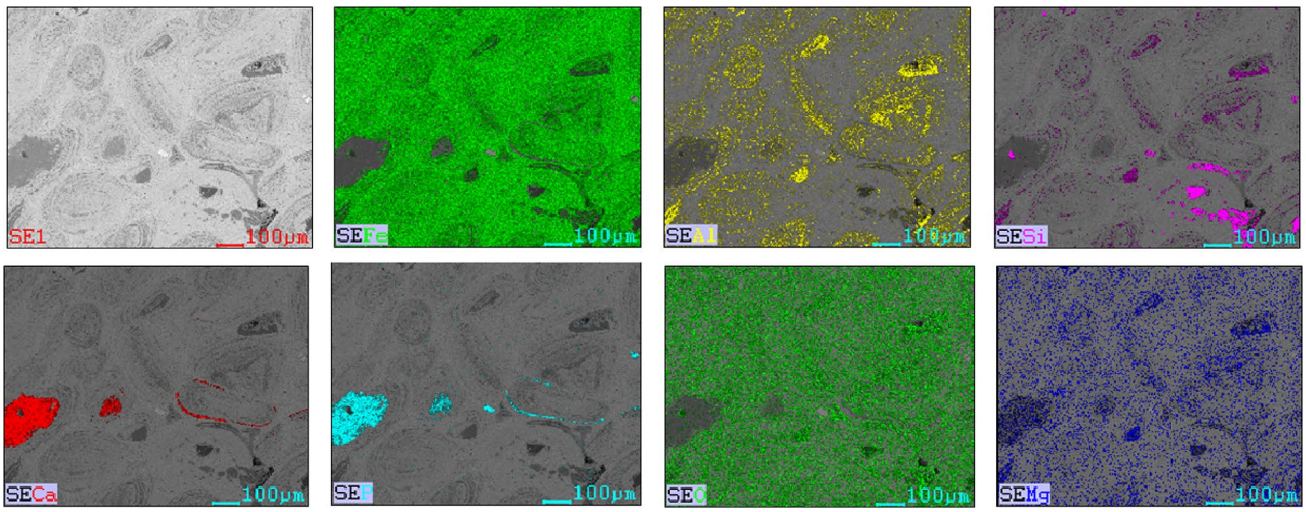

Fig. 5 Element surface scan images of iron-rich oolite and lean-iron oolite

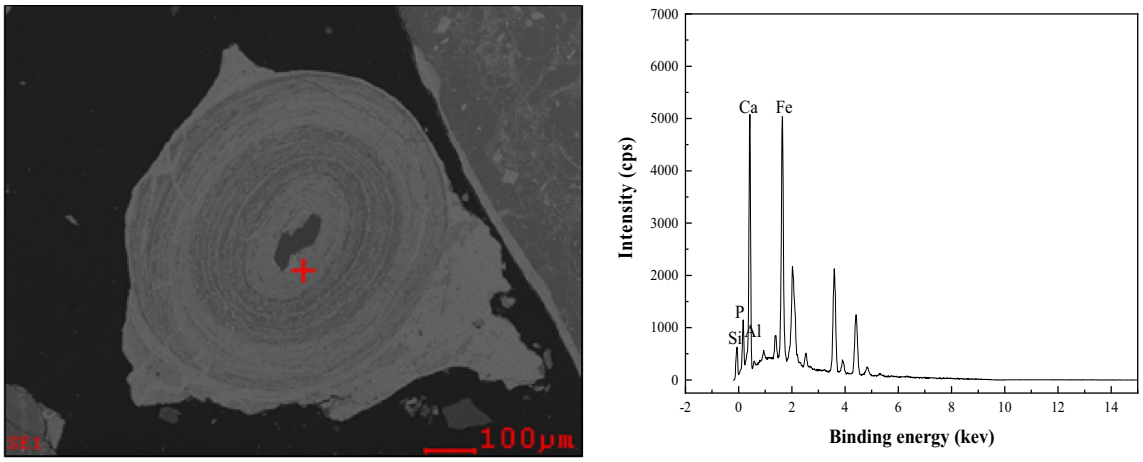

Fig. 6 SEM and EDS images of iron-rich oolite and iron-poor oolite

mineral. The mineral is black in colour with a semi-metallic lustre, and the streak is also black; it is opaque and has no cleavage. Magnetite is usually existing in the form of octahedral and rhombus dodecahedral crystals. The content of magnetite in the ores is less than 1%, which has little effect on the recovery of iron.

3.2.4 Siderite

Theoretically, siderite is composed of FeO (62.01) and CO_2 (37.99%). Iron in this mineral is often isomorphously replaced by Mg and Mn, forming magnesium magniosiderite and manganosphaerite. Iron in this mineral is sometimes replaced by calcium. In addition, impurities such as Ti, Si, Al, Ga, Zr, Co, Ba, Cd, Cu, U, P, and S may be present. Siderite may be phenocrystalline or cryptocrystalline. Phenocrystalline siderite belongs to the trigonal crystal system. Siderite is typically characterised by its colloidal, oolitic, and nodular structures, and is often associated with oolitic hematite, oolitic chlorite, and goethite. Additionally, some siderite can be found in ores.

3.2.5 Collophanite.

Under the microscope, the collophanite is light red or light brown in colour, and is non-crystalline. It is composed of colloidal, cryptocrystalline apatite. The main component of apatite is $Ca_5(PO_4)_3(OH{\cdot}F)$, which contains CaO (54.58%), P_2O_5 (41.38%), F (1.23%), Cl (2.27%), and H_2O (0.56%). Because fluorine (F) is often replaced by chlorine (Cl) or hydroxyl (OH), fluorapatite and hydrocarbon apatite can be often observed, among which fluoroapatite is the most common. The SEM images of collophanite are shown in Fig. 7. The electronic probe composition analysis

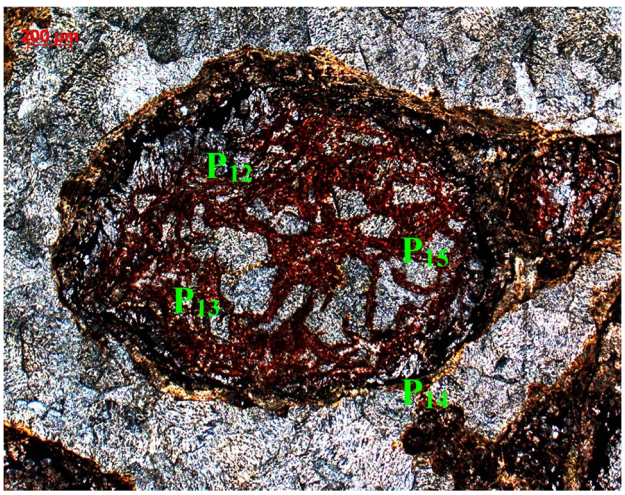

Fig. 7 SEM images of Collophanite

of collophanite (in Table 7) shows that the massive collophanite is composed of P_2O_5 (37.37%) and CaO (51.07%).

To study the distribution of phosphorus in the oolite, element scanning analysis of Fe, Si, P, Ca, and Al was performed on the particles with hematite as the main component. The positions of P and Ca matched, and were coincident with Fe, which demonstrates that the collophanite was adherent to hematite in a chimeric shape. The collophanite in ore is important because the phosphorus and sulphur in the ore are expected to be removed as harmful impurities in conventional iron-ore resources. For example, if the ore is put into a furnace for direct ironmaking using the Thomas Method without removal at the beneficiation stage, the phosphorus would become Thomas phosphatic fertiliser after being processed. For the phosphorus and sulphur, special

Table 7 Electron probe composition analysis of collophanite (wt.%)

Position	F	P_2O_5	FeO	MgO	CaO	Totals
P_{12}	4.322	37.864	0.570	0.021	50.573	93.351
P_{13}	4.889	37.825	1.420	0.033	50.690	94.858
P_{14}	4.745	38.021	0.685	0.039	50.972	94.461
P_{15}	5.682	35.770	1.117	0.061	52.047	94.678
Average	4.910	37.370	0.948	0.039	51.071	94.337

attention needs to be paid to the study of the occurrence state in ores.

3.2.6 Chlorite

The chlorite observed under the microscope is concentric oolite formed by fine phosphorus aggregates, with hematite, collophanite, and clay minerals. The colour ranges from green, greyish green, and dark green to black-green. It was green and light brown in colour under polarised light, without significant pleochroism. The chlorite is named after its structure, and its content accounts for about one-fifth of the ore. According to the element surface scan images of the chlorite shown in the oolite in Fig. 8. The position of Fe, AL, Mg, and Si in the middle of the oolite is exactly the place where the chlorite and haematite-limonite are closely associated. Eighty percent of the chlorite in the ore is associated with hematite in the form of oolite and is difficult to dissociate.

3.2.7 Feldspar and quartz

The quartz under the microscope is anhedral and fine-grained in shape, and is colourless and transparent, with angular and semi-angular structures. The positive relief is low, the maximum interference colour under cross-polarised light is level 1 yellow-white, and the uniaxial crystal is positive. The electron scan images and energy spectrum scanning results are shown in Fig. 9.

3.2.8 Dolomite, calcite, and clay minerals

Dolomite and calcite in the mining areas are sparse, and only a very small amount of calcite became the cores or

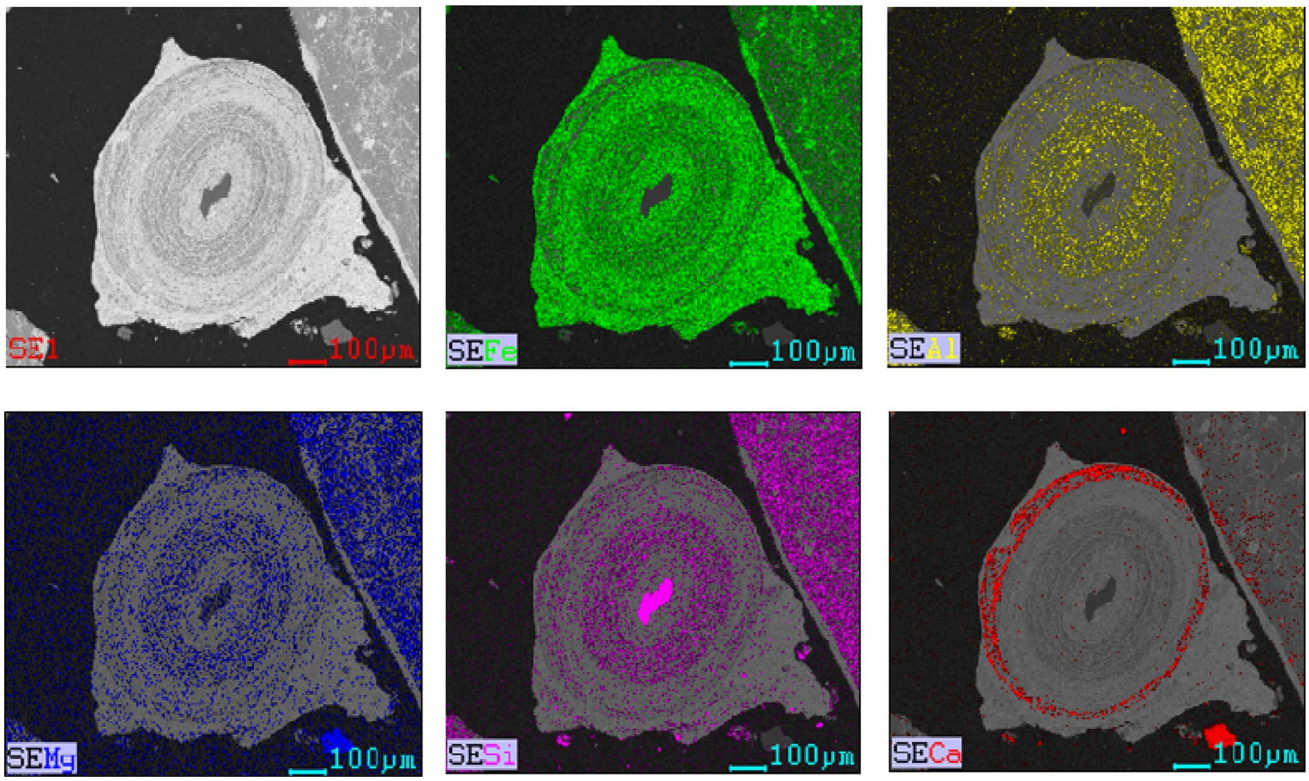

Fig. 8 Element surface scan images of chlorite in oolite

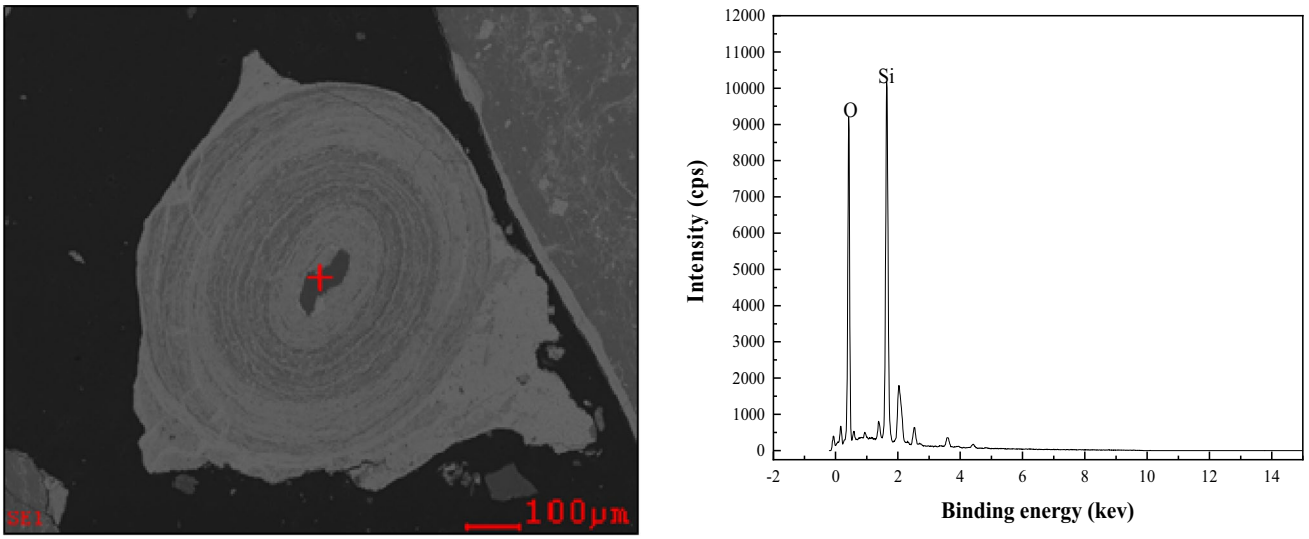

Fig. 9 SEM–EDS images of an ooid with a quartz nucleus and energy spectrum scanning results for the quartz

girdles of the hematite ooids, both of which mainly occur in cuttings and cement. Kaolin, goschwitzit, hydromica, and chlorite, collectively referred to as clay minerals, are sparse in the ore. They are distributed in the oolitic girdles with the very fine granularity of 0.1 μm, or distributed in cements containing phosphorus clay detritus.

3.3 Granularity analysis of high phosphorous ore

The main minerals in the ore (i.e., haematite-limonite, chlorite, quartz, and collophanite) are described in terms of the shape and size of individual crystals in the processing characteristics of various minerals. Seventy to eighty percent of the single crystals were unqualified because their sizes were smaller than the effective range required by mechanical beneficiation. Therefore, it is meaningless to design the mineral processing. Based on the concept of effective separation of the component aggregates from the expected mineral processing, representative ore samples have been selected. The primary granularity of the components such as oolite, cement, cuttings, collophanite, and quartz were analysed to measure the granularity of the various ore aggregates. The individual granularities of oolite, cement, cuttings, quartz, and collophanite in the ore samples are shown in Table 8. The data in Table 9 show that the granularity of the oolites, cements, and cuttings that comprise the ores in the original processing is mostly within the optimal range of mechanical beneficiation, and the original granularity of collophanite and quartz in the ores is mostly within the range of mechanical beneficiation.

In view of the process mineral characteristics of the high phosphorus iron ore, it is very difficult to extract iron and reduce phosphorus by physical separation (magnetic separation, flotation, and gravity separation). However, the effective utilization of the high iron phosphate possible realized ore effectively by pyrometallurgical dephosphorization, direct reduction roasting, suspension magnetization roasting, deep reduction roasting, and segregation roasting-magnetic separation.

Table 8 Granularity analysis results of main minerals

Classification	Range of granularity (mm)					
	0.04–0.074	0.074–0.1	0.1–0.2	0.2–0.5	0.5–1.0	>1.0
Oolite	0.73	11.25	26.58	47.65	10.54	3.25
Accumulation	100.00	99.27	88.02	61.44	13.79	0.00
Cement	20.18	29.35	26.87	11.25	6.47	5.88
Accumulation	100.00	79.82	50.47	23.60	12.35	0.00
Gangue particles/ cuttings	29.24	17.36	25.34	19.24	8.54	0.28
Accumulation	100.00	70.76	53.40	28.06	8.82	0.00

Table 9 Statistics of original processing granularity of main minerals

Classification	Range of granularity (mm)						
	< 0.04	0.04–0.074	0.074–0.1	0.1–0.2	0.2–0.5	0.5–1	> 1.0
Hematite	42.65	35.98	12.65	7.35	1.37	0.00	0.00
Accumulation	100.00	57.35	21.37	8.72	0.00	0.00	0.00
Hematite-limonite aggregates	1.54	6.58	26.87	14.57	38.99	5.43	6.02
Accumulation	100.00	98.46	91.88	65.01	50.44	11.45	0.00
quartz	13.76	26.44	28.14	18.65	7.77	5.24	0.00
Accumulation	100.00	86.24	59.80	31.66	13.01	5.24	0.00
Collophanite	23.71	31.05	25.31	14.25	5.14	0.54	0.00
Accumulation	100.00	76.29	45.24	19.93	5.68	0.54	0.00

4 Conclusions

Based on the results obtained in this work, we drew the following conclusions:

1. The high-phosphorus oolitic iron ore contained 44.70% Fe and 1.56% P in western Hubei of China. The iron-bearing chemical sedimentary minerals and ores of the high-phosphorus oolitic iron ore from western Hubei consist of oolites, cuttings, and cement. Among them, more than 60% are oolites, which are composed of an oolitic core (quartz or iron), a collophanite girdle, and a hematite girdle. The cuttings are composed of fine-grained hematite and quartz feldspar, and the cement consists of carbonate minerals and worm-like hematite.
2. The iron-bearing minerals in the oolites are mainly hematite, limonite, chlorite, and collophanite. The hematite-limonite is closely associated with iron-bearing chlorite. The electron scanning analysis results show that the electron images are consistent with the images obtained under the microscope. ($FeOOH{\cdot}H_2O$), Goethite, esmeraldite, lepidocrocite, hydrolepidocrocite, water-rich iron hydroxide gelation, aluminium hydroxides, water-containing oxides, and mud often occur together.
3. This study provides an important basis for technological mineralogy research for the selection of phosphorus extraction and phosphorus reduction processes in high-phosphorous iron ore and has important practical significance for promoting the utilization of high-phosphorous iron resources.

Funding This Project was supported by the Sichuan Science and Technology Program (2018FZ0092); the Open Foundation of the State Key Laboratory of Refractories and Metallurgy, Wuhan University of Science and Technology (ZR201801).

Compliance with ethical standards

Conflict of interest On behalf of all authors, the corresponding author states that there is no conflict of interest. The funders had no role in the design, analyses, and interpretation of any data of the study.

References

1. Bonazzi P, Bindi L, Medenbach O, Pagano R, Lampronti GI, Menchetti S (2007) Olmiite, $CaMn[SiO_3(OH)](OH)$, the Mn-dominant analogue of poldervaartite, a new mineral species from Kalahari manganese fields (Republic of South Africa). Mineral Mag 71(2):193–201
2. Garnit H, Bouhlel S (2017) Petrography, mineralogy and geochemistry of the Late Eocene oolitic iron stones of the Jebel Ank Southern Tunisian Atlas. Ore Geol Rev 84:134–153
3. Viktor J, Ferenc M, Buchs D, Peter K (2012) The connection between iron ore formations and"mud-shrimp" colonizations around sunken wood debris and hydrothermal sediments in a Lower Cretaceous continental rift basin Mecsek Mts. Hungary. Earth Sci Rev 114(3–4):250–278
4. Mukhtar AA, Mukhymbekova MK, Makashev AS, Savin VN (2018) Thermomagnetic enrichment and dephosphorization of brown iron ore and concentrates. Steel Transl 48(9):553–557
5. Liu SX, Lu XL, Niu FS (2003) The present conditions of micro-fine disseminated refractory oolitic hematite and expectation. Adv Mater Res 734–737:211–214
6. Liu X, Li C, Luo H, Cheng R, Liu F (2017) Selective reverse flotation of apatite from dolomite in apatite ore using saponified gutter oil fatty acid as a collector. Int J Miner Process 165:20–27
7. Boucher D, Deng Z, Leadbeater TW, Langlois R, Waters KE (2015) Speed analysis of quartz and hematite particles in a spiral concentrator by PEPT. Miner Eng 91:86–91
8. Cowan CA, James NP (1992) Diastasis cracks: mechanically generated synaeresis-like cracks in Upper Cambrian shallow water oolite and ribbon carbonates. Sedimentology. 39(6):1101–1118
9. Dill HG, Botz R, Berner Z, Stüben D, Nasir S, Al-Saad H (2005) Sedimentary facies, mineralogy, and geochemistry of the sulphate-bearing Miocene Dam Formation in Qatar. Sediment Geol 174(1–2):63–96
10. Xiao JH, Zhou LL (2019) Increasing iron and reducing phosphorus grades of magnetic-roasted high-phosphorus oolitic iron ore by low-intensity magnetic separation–reverse flotation. Processes 7:388

11. Kholodov VN, Nedumov RI, Golubovskaya EV (2012) Facies types of sedimentary iron ore deposits and their geochemical features: Communication 1. Facies groups of sedimentary ores, their lithology, andgenesis. Lithol Miner Resour 47(6):447–472
12. Kimberley MM (1974) Origin of iron ore by diagenetic replacement of calcareous oolite. Nature 250(5464):319–320
13. María SR, Lucía E, Gómez P, Krause JM, Matheos SD (2014) Controls on clay minerals assemblages in an early paleogene nonmarine succession: Implications for the volcanic and paleoclimatic record of extra-andean patagonia, Argentina. J S Am Earth Sci 52(1):1–23
14. Pearce M, Nicholas A, Timms E (2013) Reaction mechanism for the replacement of calcite by dolomite and siderite: implications for geochemistry, microstructure and porosity evolution during hydrothermal mineralisation. Contrib Mineral Pet 166(4):995–1009
15. Liu F, Zhang W, Xing HW (2014) Effects of fuel on gasification dephosphorization of high-phosphorus oolitic hematite ore. Adv Mater Res 881–883:1536–1539
16. Li YL, Sun TC, Kou J, Xu CY, Liu ZH, Guo Q (2012) Industry test on phosphorus removal and direct reduction of high-phosphorus oolitic hematite ore. Adv Mater Res 402:535–541
17. Liu ZJ, Xing XD, Zhang JL, Cao MM, Jiao KX, Ren S (2012) Reduction mechanisms of pyrite cinder-carbon composite pellets. Int J Miner Metall Mater 19(11):986–991
18. Markl G, Blanckenburg FV, Wagner T (2006) Iron isotope fractionation during hydrothermal ore deposition and alteration. Geochim Cosmochim Acta 70(12):3011–3030
19. Yu JW, Han YX, Li YJ, Gao P (2019) Recent advances in magnetization roasting of refractory iron ores: a technological review in the past decade. Miner Process Extract Metall Rev. 2:5. https://doi.org/10.1080/08827508.2019.1634565
20. Zhang JS (2007) Status and trend of exploitation and utilization of iron ore resources in China. China Metall 17(1):1–6 **(in Chinese)**
21. Sun WH, Wu P, Zhang L (2015) Geological characteristics and metallogenic analysis of Liujiawan iron ore deposit in badong county Hubei province. Resour Environ Eng 29(04):387–390 **(in Chinese)**